Models for the marine Mo cycle

In what follows we describe our Mo isotope mass balance and some of the considerations in building and evaluating it. We model the Mo isotope composition of seawater through time by first considering the modern system. As described in the text, Mo is buried into three categories of sinks: 1) deep oxic sediments (OX) 2) sulfidic shelf sediments underlying O_2 poor waters (SAD) and 3) euxinic sediments (EUX). In many oxic sediments, no authigenic Mo accumulation is observed and, hence, they do not contribute to the overall Mo budget (e.g. Baja, Mexico (1), Mid-Atlantic (2), Japan Sea, Arabian Sea (3) Washington State margin (4)). Therefore, the three sinks account for all authigenic Mo removal, but do not cover the entire seafloor.

Mo geochemistry

The geochemical behaviour of Mo is determined by the presence of dissolved H_2S and O_2 in aqueous solution. In oxic waters, Mo is soluble and exists as the molybdate anion, MoO_4^{2-}. Removal of Mo under oxic conditions occurs slowly as a rare species, $Mo_6O_{19}^{2-}$, adsorbs onto Mn-oxides (5), and in modern, well oxygenated oceans, this oxic pathway accounts for 35-50% of Mo removal (Table S3). In sulfidic waters, molybdate reacts with H_2S to form particle reactive oxythiomolybdates, $MoO_{4-x}S_x^{2-}$ (x = 0, 1, 2, 3, 4) (6), which are scavenged when H_2S > 11 mM or total sulfide ($S^{2-} = H_2S + HS^- + S^{2-}$) > 25 mM at pH levels typical of sulfidic environments. Where sulfide is present in the water column (euxinic settings) or in pore fluids, Mo accumulates at a 100-1000 fold higher rate than when sulfide is absent (7).

Isotope fractionation in the modern ocean

Ferromanganese crusts and nodules deposited below ~1000m depth constitute the oxic Mo sink (OX) imparting strong fractionation during the Mo adsorption process, $\Delta_{SW\text{-}OX}$ = 2.8±0.1‰ (Figure S1, Table S2). In shallower settings with oxygen-poor bottom waters, Mo accumulates in sediments when sulfide is available in pore fluids for oxythiomolybdate formation (8). These settings are found in modern oxygen minimum zones and other low oxygen water masses (SAD), this removal pathway imparts a smaller fractionation, $\Delta_{SW\text{-}SAD}$ = 0.7±0.2‰ (9). Under highly euxinic conditions (EUX) with H_2S > 11 mM in pore fluids or in the water column, Mo is rapidly converted to particle reactive species and quantitatively scavenged without isotope fractionation from seawater (10) (Table S2). However, in mildly or intermittently euxinic basins, where H_2S concentrations < 11 µM, isotope fractionation is comparable to that seen in shallow sulfidic sediments(10, 11).

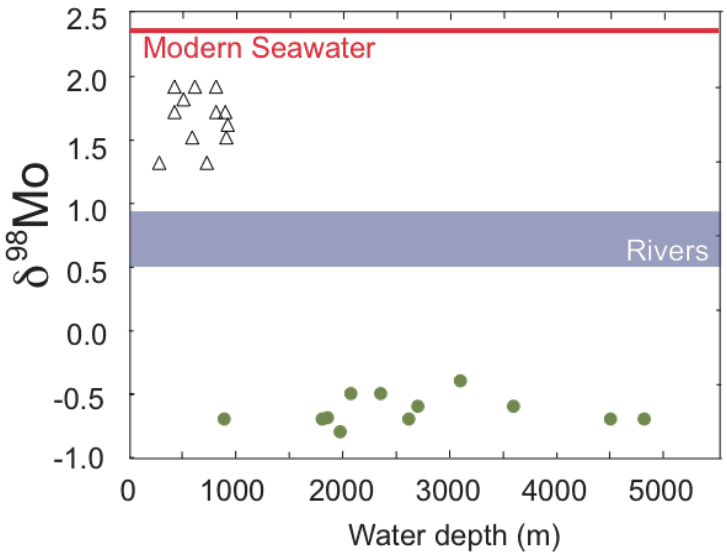

Figure S1: δ^{98}Mo in modern marine sediments versus water depth with ferromanganese crusts (●) and sediment deposited in oxygen-poor waters (△). Isotopic composition of the deepest sample in each core is shown. Non-steady state systems are not shown (see Table S2).

Table S2: Sedimentary δ^{98}Mo in modern marine sediments from 47 locations.

Location	Core Name	Water Depth	Core depth	$[Mo]_{auth}$ top	δ^{98}Mo top	$[Mo]_{auth}$ bottom	δ^{98}Mo bottom	Refs
		m	cm	ppm	‰	ppm	‰	
			Oxic-deep					
Atlantic Deep	BM 1969.05	1800	62 Myr	7	-0.6	400	-0.7	(12)
Atlantic Deep	63-43DS, SO-84	1970	Surface	239	-0.8	-	-	(12)
Atlantic Deep	1965.0.35, Atlantis II	878	Surface	307	-0.7	-	-	(12)
Pacific Deep	44-8KD	2615	Surface	459	-0.7	-	-	(12)
Pacific Deep	31-22KD	2350	Surface	277	-0.5	-	-	(12)
Indian Deep	51-113D-D	4513	Surface	496	-0.7	-	-	(12)
Indian Deep	50-145D-C	2700	Surface	296	-0.6	-	-	(12)
Pacific Deep	237KD	4830	Surface	414	-0.6	435	-0.7	(12)
			Oxic – deep with Mo loss					
			(Mo release by reductive dissolution of Mn-oxides. Possibly preserved by sulfide capture.)					
East pacific Deep, Central America	Manop H	3600	20	55	-0.5	5.6	-0.6	(9)
East pacific, California	San Clemente	2070	24	32.4	-0.2	0.2	-0.5	(13)
East pacific - deep	Manop M	3100	18	15	-0.2	0.6	-0.4	(9)
Mediterranean Sea [a)]	BP018BC	1850	27	345	-0.25	7.4	-0.69	(14)
Mediterranean Sea [a)]	SL114	3390	32-34	26.9	-1.1	23	-0.82	(14)
			Transient systems					
			(possibly changing from Mn-oxide dominated to non-ventilated bottom waters with sulfide availble)					
East pacific, California	Sta Catalina	1301	39	0.8	2.2	1.5	-0.2	(9)
East pacific, California	Sta Nicolas, CA	1750	33	1.6	0.5	1.2	-0.4	(9)
East pacific, California	Tanner Basin, CA	1514	21.5	2.2	1.2	6.1	0.3	(13)
			Oxic-shelf (SAD)					
			(Preservation in sulfidic pore waters)					
East pacific, California	Santa Barbara, MC17	493	41	3.7	1.4	3.8	1.8	(9)
East pacific, California	Sta Monica 2	910	6.9	2.6	1.6	3.3	1.6	(9)
East pacific, Mexico	Magdalena	713	8.3	4.5	1.9	12	1.3	(9)
East pacific, Mexico	Alfonso 1	408	50.5	6.1	2	10	1.9	(9)
East pacific, Mexico	La Paz	887	6.5	5.6	2.1	8.5	1.7	(9)
East pacific, Mexico	Alfonso 2	408	6.5	6.5	1.9	11	1.7	(9)

East pacific, Mexico	Pescadero 1	600	11.8	1.8	2.7	2	1.9	(9)
East pacific, Mexico	Carmen 1	800	9.1	4.4	1.8	7.1	1.9	(9)
East pacific, Peru	Peru	264	33	87	1	37	1.3	(9)
East pacific, Mexico	Pescadero 2	800	11.8	2.2	2	2.2	1.7	(9)
East pacific, Mexico	Carmen 2	575	9.1	4.6	1.4	5.3	1.5	(9)
East pacific, Mexico	Mazatlan		59	5.6	1.6	14	1.6	(15)
East pacific, California	San Pedro	897	34.8	10.3	1.8	1.7	1.5	(13)
East pacific, California	Sta Monica 1		24	1.1	1.4	4.4	1.3	(13)
East pacific, Mexico	San Blas		47.8	4.4	1.8	13	1.6	(15)
East pacific, Mexico	Soledad		46.5	3.4	1.6	9.7	1.7	(15)
			Euxinic – mild (H_2S <11 mM)					
	Site 1002, ODP							
Cariaco Basin	leg 165	900	600-640	95	1.79	192	1.76	(11)
Black Sea	7613-1	84	Surface	5.0	-0.06	-	-	(10)
Black Sea	7614-1	91	Surface	2.9	0.24	-	-	(10)
Black Sea	7611-1	130	Surface	1.0	0.53	-	-	(10)
Black Sea	7615	148	Surface	2.1	0.84	-	-	(10)
Black Sea	7612-3	188	Surface	17.8	-0.13	-	-	(10)
Black Sea	24 MUC 1	207	Surface	28.5	-0.63	-	-	(10)
Black Sea	14 MUC 7	272	Surface	46.1	0.36	-	-	(10)
Black Sea	station 6	396	3-4	51.8	0.36	-	-	(10)
Black Sea	25 MUC 1	410	Surface	67.7	1.64	-	-	(10)
Baltic Sea, Gotland								(10)
Deep	48/1 GD	168	0-1.6	90	0.57	-		
Baltic Sea, Gotland								(10)
Deep	271-2-GD	247	1.8	191	0.41	-		
Baltic Sea, Landsort								(10)
Deep	36/1 LD	450	0-1.6	115	0.11	-		
			Euxinic (H_2S > 11 mM)					
Black Sea	17 MUC 4	500	Surface	52.5	2.24	-		(10)
Black Sea	7618-3	943	Surface	49.4	1.95	-		(10)
Black Sea	7619-1	1246	4-5 cm	32.5	2.44	-		(10)
Black Sea	7606-2	1800	5-10 cm	33.7	2.08	-		(10)
Black Sea	7620-1	2002	5-6 cm	25.9	2.07	-		(10)
Black Sea	7620-3	2055	2-3 cm	25.8	2.10	-		(10)

[a)] The Mediterranean sediment cores experienced diagenetic overprint and show atypical Mo isotopic compositions (14).

Paleo-ocean isotopic Mo budget

The isotopic composition of seawater ($\delta^{98}Mo_{SW}$) serves as a measure of the relative proportions of the molybdenum sink in the ocean at any given time in Earth's history. In its modern oxic state, the ocean is strongly enriched in ^{98}Mo due to a large fractionation resulting from Mo removal into oxic sediments. At times of expanded sulfide inventory in the oceans, the overall Mo removal would be more efficient, driving oceanic Mo inventory down, and net isotope fractionation becomes small. The model derived here is dedicated to the long-term changes in the Mo isotopic record at times when the system is in steady state. We first outline the theoretical framework by which Mo isotopic composition of seawater change, and subsequently discuss model assumptions, constraints and how data from the sedimentary record constrain the model.

Isotope balance in the ocean is mainly established between oxic (large fractionation) and euxinic sinks (small fractionation):

(2) $$\delta_{IN} = f \cdot \delta_{Non\text{-}EUX} + (1\text{-}f) \cdot \delta_{EUX}$$

Here, f is the fraction of the Mo output buried in both deep oxic sediments (OX) and sulfidic sediments (SAD). The isotopic composition of the fractionated, non-euxinic sink ($\delta_{Non\text{-}EUX}$) is given by the weighted average of fully oxygenated deep sediments (OX) and shallow sediments with oxygen poor bottom water where sulfide precipitates at depth (SAD) with g defining the deep oxic fraction of non-euxinic sinks:

(3) $$\delta_{Non\text{-}EUX} = g\ \delta_{OX} + (1\text{-}g)\ \delta_{SAD}$$

A net isotopic offset from overlying seawater can result during burial into both types of sediments, but importantly fractionation always proceeds towards lighter isotope compositions in the products: $\delta_{OX} = \delta_{SW} - \Delta_{OX}$, $\delta_{SAD} = \delta_{SW} - \Delta_{SAD}$ and $\delta_{EUX} = \delta_{SW} - \Delta_{EUX}$ (Δ are all positive numbers, details below). In combination with equations 2 and 3, the isotopic composition of seawater yields:

(4) $$\delta_{SW} = \delta_{IN} + (1\text{-}f) \cdot \delta_{EUX} + f \cdot g \cdot \delta_{OX} + f \cdot (1\text{-}g) \cdot \delta_{SAD}$$

Seawater isotope composition is a function of six parameters of which two (f and g) are variables between 0 and 1, three fractionation factors and with the isotope composition of the source input as a boundary condition. If we keep fractionation factors at their modern value, so that Δ_{OX} = 2.8±0.1‰(12, 16, 17), Δ_{SAD} = 0.7±0.2‰ (9, 13, 15) and Δ_{EUX} = 0.0‰ (10), δ_{SW} becomes a function of input and the relative proportions buried in the three settings can be derived, see Figures 2, S2 and S3.

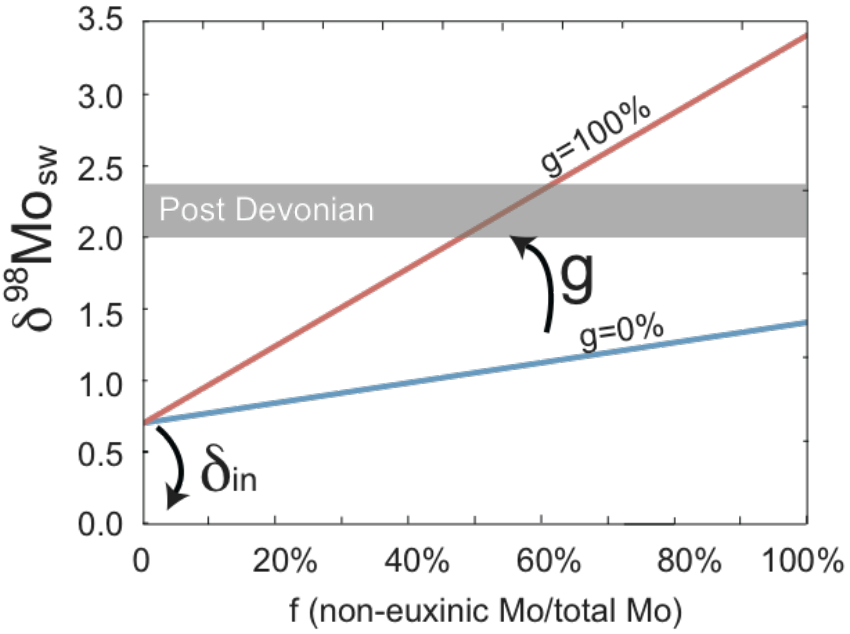

Figure S2: $\delta^{98}Mo_{SW}$ is a function of the oxic removal fraction, f. The effects of oxic removal in deep ocean, g, and input composition, δ_{in}, are shown.

Scott et al. estimates the modern oceanic elemental and isotopic Mo budget suggest that the ocean is balanced by these three sinks (Table S2), with deep oxic, sulfidic sediments, and euxinic sediments accounting for 35%, 50% and 15% of the total oceanic removal, respectively (7). Other estimates suggest lower euxinic proportions (5%) because intermittently euxinic upwelling zones are not included in the euxinic sink (9, 18).

Table S3: Recent estimates for the relative proportions of modern Mo sinks and its corresponding parameterization in terms of f = OX/[OX + SAD +EUX] and g = OX/[OX+SAD}.

Source	Oxic deep	Oxic shallow "suboxic"	Euxinic	f	g
Scott et al. 2008	35%	50%	15%	0.85	0.41
Brucker-Poulson et al. 2009	50%	45%	5%	0.95	0.53
Kendall et al. 2009	35%	60%	5%	0.95	0.37
Range	35-50%	45-60%	5-15%	0.95	0.37

Model assumptions

Mo residence time

We assume that the Mo cycle is in steady state and that the Mo inventory is large enough that surface waters are well-mixed with respect to Mo and carry a homogeneous δ^{98}Mo composition.

If overall removal rates are fast in any given basin (or in the entire ocean), the Mo isotope composition may vary within that body of water (ocean). For example, this would be expected in a fully euxinic ocean. We must, therefore, require both that samples were deposited in a basin that did exchange water with the open ocean, and that the oxic surface waters are well mixed with respect to Mo. That is, the Mo residence time in the ocean is much longer than ocean mixing time scales. The Black Sea offers a modern example with rapid Mo removal due to its strongly euxinic bottom waters, yet surface waters carry oceanic molybdenum with δ^{98}Mo = 2.3‰ (10, 14).

When is then the ocean no longer well-mixed with Mo? Based on the Mo/TOC proxy, Scott et al. (2008) estimates the oceanic Mo inventory to <5 nM, <21 nM and >>21 nM

in the Archean, Proterozoic, and Phanerozoic, respectively (7). At the modern riverine discharge rate and steady state, this corresponds to a Mo residence time of <35, <150 and <730 kyrs. If this interpretation is correct, Mo would have been well mixed in early Paleozoic oceans.

The constantly high δ^{98}Mo > 1.5‰ in the ca. 392-365 Ma in Mid- to Upper Devonian shales provides independent evidence that Mo was well mixed in the ocean at this time, since the large fractionation is generated in the deep oceans by precipitation of ferromanganese oxides. Thus, the studied basins must, therefore, have exchanged water with the deep ocean.

Local restriction

At lower oceanic Mo inventory, the riverine Mo fraction in restricted basins would increase compared to Mo derived from seawater, and average δ^{98}Mo discharge to such basins would fall closer to riverine values. This effect has been suggested to account for d^{98}Mo variability in the Toarcian OAE(19). To quantify the potential of this isotope dilution, we can look at the modern Black Sea - a highly restricted basin. Water is supplied into the basin from rivers and seawater through the Bosporus Strait in roughly equal proportions(20). Today Mo concentrations in seawater is ~20 times higher than in rivers (105nM compared to 6 nM), giving average water supply to the basin an isotopic composition shifted by -0.08‰ relative to seawater.

Riverine Mo flux

Molybdenum is transported in solution as molybdate ion after chemical weathering of continental rocks. It is not clear if this process would accelerate during rises in the O_2 concentrations Neoproterozoic and Phanerozoic atmospheres which were already oxic (likely pO_2 > 1-3% (21)). A change in source flux can hypothetically change the proportions of Mo buried in various environments, if removal rates in the major sinks do not respond in a proportional manner when the Mo inventory decrease.

Riverine $\delta^{98}Mo$

Today, Mo is delivered mainly through rivers (~90%) with a small contribution from hydrothermal sources (~10%) (22). The isotope composition of average riverine discharge is $\delta^{98}Mo = 0.7\pm0.1‰$ (23) largely determined by the discharge of the Amazon river (81% of the analyzed water supply) with considerable variation in smaller rivers. Hydrothermal vents is taken to supply Mo at a similar composition ~0.8‰ (24), but so far only one hydrothermal vent system has been analyzed. The oceanic input is heavier than crustal rocks represented by granites and clastic sediments, 0.15±0.15‰ 1sd n = 4 (12), but within the wide range observed in molybdenite deposits 0.39±0.56‰, 1sd n = 54 (25-27)[1]. It has been proposed that isotope fractionation can occur during weathering and/or transport into rivers by the retention of light Mo in soils (23). If this process changed in time, it may change the quantitative interpretation (f, g) as well. However, increasing $\delta^{98}Mo_{IN}$ with time is most unlikely to explain the systematic increase in $\delta^{98}Mo_{EUX}$ maxima over time, because it requires a highly fractionated Mo reservoir to build up on land (isolated from weathering).

Fractionation factors

The molecular-scale mechanisms driving fractionation is understood for the oxic burial pathway where adsorption occurs between an octahedrally coordinated polymolybdate anion ($Mo_6O_{19}^{2-}$) and birnessite (5). The observed isotope fractionation results from equilibrium reactions with polymolybdate being 2.7‰ lighter than the dominant Mo species in oxic waters, molybdate(5). This isotope offset is constant at relevant seawater temperatures and ionic strengths(16) which justifies keeping Δ_{OX} constant in time.

Mo isotope fractionation can also occur during adsorption onto iron oxides with substantial isotope fractionation -0.6 to -2.2‰ depending on the oxide compound (28). However, the importance of this removal pathway in the ocean still remains unclear.

[1] The comparisons are performed without a universal reference. It does not change the overall patterns since in-house standards so far agree at the <0.1‰ level.

Fractionation in sulfidic systems is currently based on empirical observations of modern marine sediments (Table S2). Our data compilation supports that fractionation can occur in systems where oxygen is intermittently present at the sediment surface. The mean isotope fractionation associated with sulfidic sediments and mildly or intermittently euxinic settings might well have been the same in the early Paleozoic as today (Figure 1). It is possible that the euxinic sink is generally associated with isotope fractionation (because highly euxinic settings always imply some mildly euxinic settings higher in the water column). However, model results differ only slightly when we allow fractionation of -0.5‰ in the euxinic sink (Figure S3).

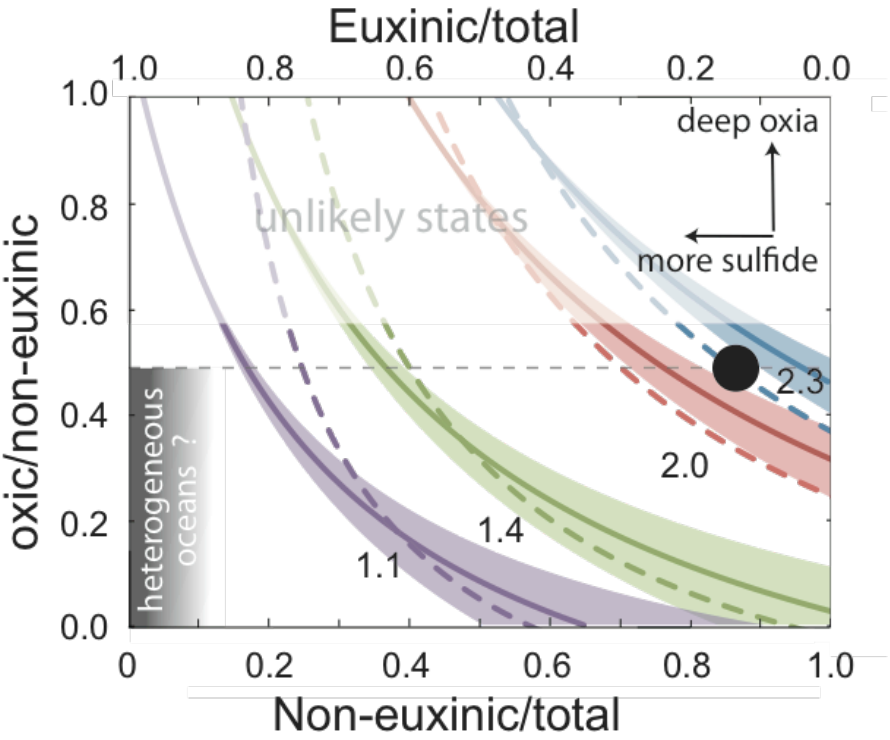

Figure S3: Model results showing the ocean states consistent with $\delta^{98}Mo_{SW}$ inferred from our data with average fractionation of Δ_{EUX} = 0.5‰ (solid lines) and shaded regions representing ±0.2‰ uncertainty of Δ_{SAD}. Dashed curves represent Δ_{EUX} = 0‰ (as in Figure 2).

Representative sampling

Much attention has been paid to geological successions where the oceanic redox conditions are known to have changed; for example during oceanic anoxic events at the Precambrian-Cambrian boundary, the Cambrian SPICE event, and the Toarcian anoxic event. During these anoxic events, the oceanic molybdenum cycle is obviously not in steady state and Mo isotope compositions change in response to both local and global conditions, so how do we know that the highest δ^{98}Mo value actually represents global seawater and not some transient state where ^{98}Mo were accumulating in the ocean? Here, we need to think about what causes global positive excursions: ^{98}Mo enrichment is caused by oxygenation, which means that positive excursion is potentially caused by a transient oxic ocean state, but reality tells us that the events were all transiently more anoxic. Instead, we suggest that quantitative removal (no fractionation) is often linked to peak of these events and these record 'global' seawater. To circumvent this bias, we have chosen to include samples from times when the ocean redox chemistry is not thought to change.

Separating global and local signals in sediments

We utilize Fe based proxies to determine the local redox conditions and determine Mo isotope composition of the euxinic samples where the probability of getting seawater value is maximal.

Fe^{2+} is transported in solution only under anoxic waters. This transport mechanism leads to enrichments of highly reactive iron relative to total iron. Riverine particulates have $Fe_{HR}/Fe_T < 0.38$ (29), and higher values indicate anoxic basins. In euxinic basins, H_2S occurs in excess over Fe^{2+} and most of the highly reactive iron is converted to pyrite: $Fe_P/Fe_{HR} > 0.7$. The threshold value has not been calibrated in modern sediments and some authors are using a threshold of >0.78 or >0.80 (30, 31) to decide euxinic conditions. The degree of pyritization DOP = Fe_P/Fe_{HCl} has been calibrated and >0.75 is diagnostic of euxinic basins, while some euxinic basins are overlooked, at DOP = 0.6-

0.75, when the value is reduced by HCl-reactive silicate phases that were unreactive towards sulfide on short diagenetic time scales (29). A threshold of 0.75 would be conservative, but we choose $Fe_P/Fe_{HR} > 0.70$ to include our highest Devonian $\delta^{98}Mo$ value at 1.93‰.

Samples classified as euxinic sediments are typically enriched in Mo with concentrations in the 10-100 ppm range except when the Mo concentration in the basin (ocean) was particularly low. In this case, bulk $\delta^{98}Mo$ in samples must be interpreted with caution, since detrital material can then contribute significantly. Accordingly, we define samples with significant detrital component as detrital: Mo EF > 2 or $Mo > 2*Mo_{detrital} = 3$ ppm (Figure 1 and 3).

Statistical significance of the δ^{98}Mo and Mo/TOC records

The apparent increase in sedimentary $\delta^{98}Mo$ and Mo/TOC has led us to hypothesize that ocean redox chemistry changed during two episodes of oxygenation when large motile animals emerged ~542 million years ago, and in the Early Devonian ~ 390 million years ago when vascular plants invaded land. Here, we present statistical tests to show that the elemental and isotopic records are truly distinct in these intervals, and an evaluation of the confidence that early Paleozoic oceans had a distinctly lower $\delta^{98}Mo$ than later Phanerozoic oceans.

We know from first principles that both Mo concentration and $\delta^{98}Mo$ in sedimentary rocks is always limited to a maximum value given by Mo concentration and $\delta^{98}Mo$ of seawater. It is therefore the maximum value in the sedimentary record that best constrains the composition of contemporaneous seawater. However, all samples are deposited from seawater and carry a signal of seawater. In order to extract this information we look at the histograms and derive a probability distributions of the Mo records that we can comopare for each time stage (Figure S4, Figure S5).

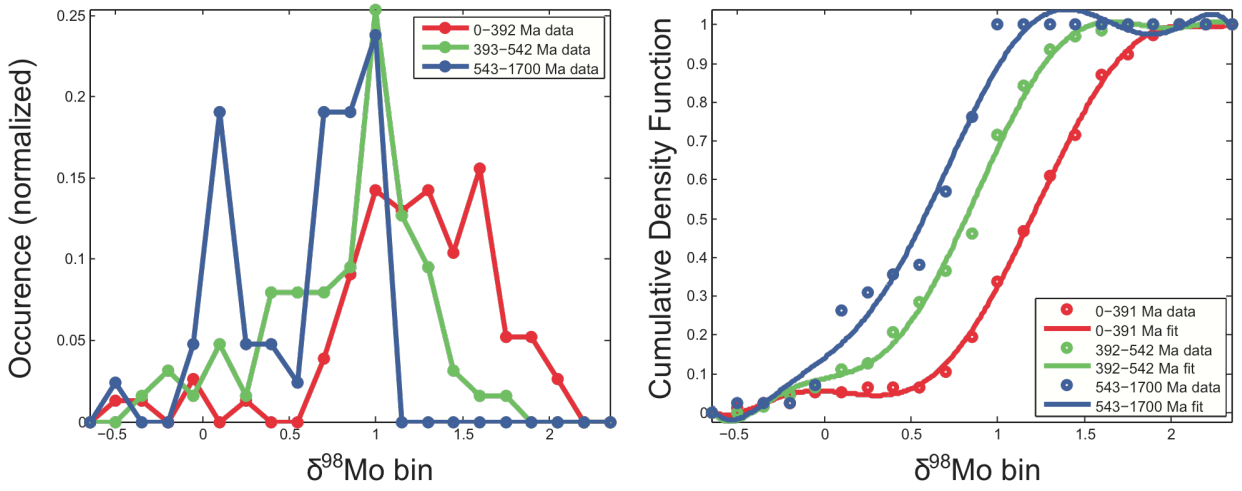

Figure S4: a) Normalized histogram for the δ^{98}Mo records and b) cumulated histogram with fitted polynomials representing the cumulative density function (CDF). See legend for details.

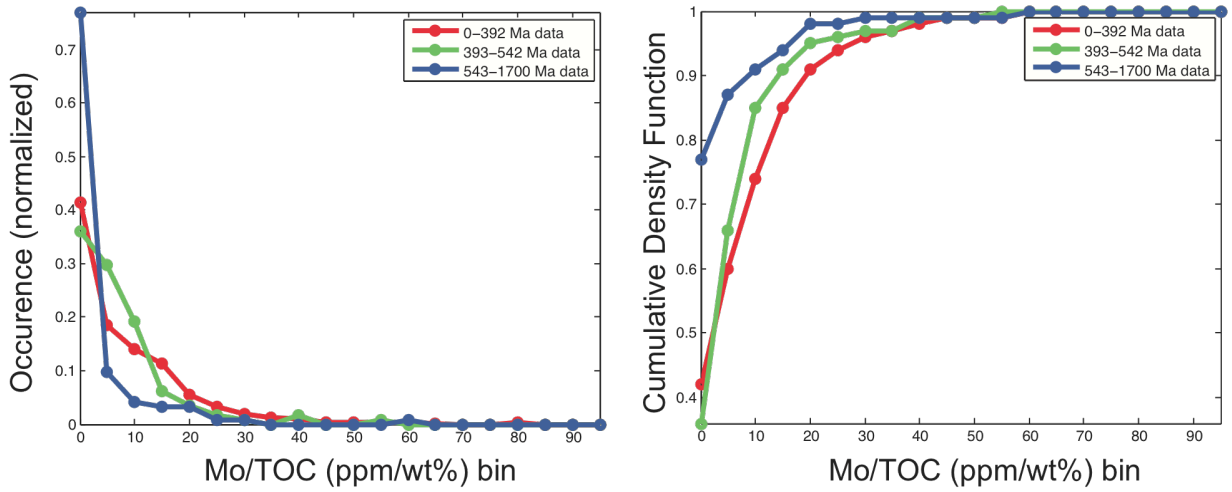

Figure S5: a) Normalized histogram of the Mo/TOC records and b) cumulated histogram with fitted polynomial representing the cumulative density function (CDF). See legend for color code.

The steady increase with time of the 90-percentile levels (Table S4) for the sediment data is best explained by an overall enrichment with time of Mo and $^{98}Mo/^{95}Mo$ in ocean water.

Table S4: 90-percentile levels of the Mo/TOC and $\delta^{98}Mo$ records. Only samples with TOC >0.5wt% are included in this calculation to avoid unrealistic Mo/TOC for samples with negligible TOC content that was most likely deposited in non-euxinic environments. Modern samples are excluded.

Time interval 90%-tile	**Mo/TOC (ppm/wt%)**	**$\delta^{98}Mo$ (‰)**
543-1800 Ma	10 (n = 739)	1.10 (n = 74)
392-542 Ma	19 (n = 123)	1.37 (n = 50)
0-391 Ma	24 (n = 114)	1.84 (n = 32)

We correct for oversampling in younger intervals by bootstrapping the observed records, and randomly sample a set of ~half the total number of samples in the smallest interval (16 for $\delta^{98}Mo$) 10,000 times and compute maximum value and its standard deviation (Table S5). The maximum value obtained from the isotope data is distinct in each interval and show much less variability than for elemental data.

Table S5: Maxima values of Mo/TOC and $\delta^{98}Mo$ distributions functions (Figure S4) when subsampled 10,000 times in portions of 57 and 16 samples, respectively. Errors represent 1 s.d. levels,

Sedimentary rocks Max (bootstrap)	**Mo/TOC (ppm/wt%)**	**$\delta^{98}Mo$ (‰)**
543-1800 Ma	41±17	1.1±0.0
392-542 Ma	43±11	1.5±0.2
0-391 Ma	53±16	2.0±0.1

Is the maximum $\delta^{98}Mo$ value of Early Paleozoic sediments distinctly lower than

equivalent later Phanerozoic sediments? To test this we assume the opposite hypothesis is true: The true Early Paleozoic sedimentary δ^{98}Mo distribution is identical to the Late Phanerozoic distribution, but sparse sampling have given us a lower maxima value. The probability that this hypothesis is true is calculated by randomly sampling the cumulative density function (CDF) of the Phanerozoic distribution in chunks of 50 samples many times and sort the results after maximum value (Figure S5). The resulting distribution shows that a δ^{98}Mo maximum of 1.6‰ will randomly occur in 0.03% of cases - and we reject the hypothesis. One sample in the Early Cambrian Niutitang Fm is found at 1.89‰. If we allow this sample to represent seawater value between 542 Ma and 390 Ma, we can only reject the hypothesis with 66% confidence. However, we notice that persistently high δ^{98}Mo values, ~1.6-2.0‰ is only found in Devonian successions (see details in a subsequent section) whereas most older succession display lower values. We will not exclude the possibility that oceans experienced a transitory period of oxygenation at the very beginning of the Phanerozoic. More samples from the late Ediacaran will tell.

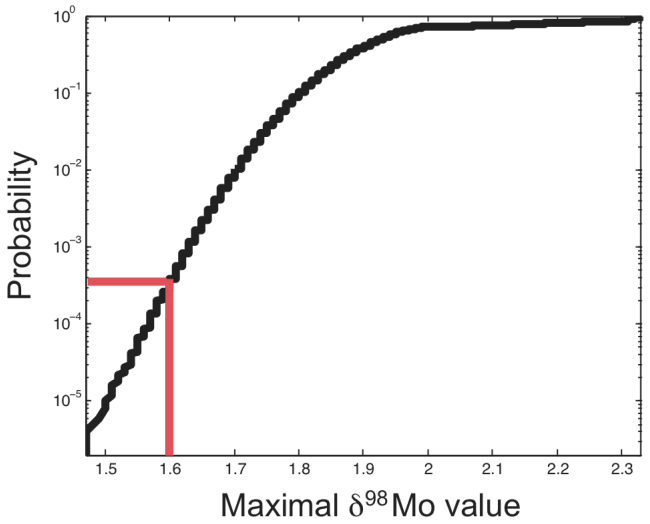

Figure S6: Probability of finding a maximum δ^{98}Mo value of $\delta^{98}Mo_{max}$ when randomly picking 50 samples (= number of samples in early Paleozoic interval) from the Phanerozoic CDF (Figure S4). An early Paleozoic maximum value of 1.6‰ is distincly

lower than what would be sampled from the Later Phanerozoic distribution with 99.97% confidence.

Hypoxia tolerance in modern fish

Fish are more sensitive to reduced oxygen concentrations than other marine animals (e.g. crustaceans, annelids and bivalves) (33) and their presence may serve as a proxy for high oxygen levels in a given environment. Prolonged exposure to 90-125 μM O_2 (30-40% PAL, present atmospheric level) cause acute mortality in many fish species (33, 34). Figure S7 summarize the measured hypoxia tolerance versus maximal fish length. The largest species tend to have the highest O_2 demand, perhaps due to higher resting metabolic rate (35), active metabolic rate (36) and oxygen consumption in fish with larger body size. There is considerable variation within experiments of the same species and between species possibly related to changes in stage of life cycle, life style, and environmental conditions (e.g. optimal temperature). However, the appearance of meter-sized, jawed fish in the Early Devonian (37) marks a six orders magnitude increase (!) in body weight compared to centimeters sized, jawless fish of the earlier Paleozoic (38). This transition suggests that minimum allowable O_2 levels increased from ~20% present atmospheric level (early Paleozoic) to ~50% PAL (Devonian).

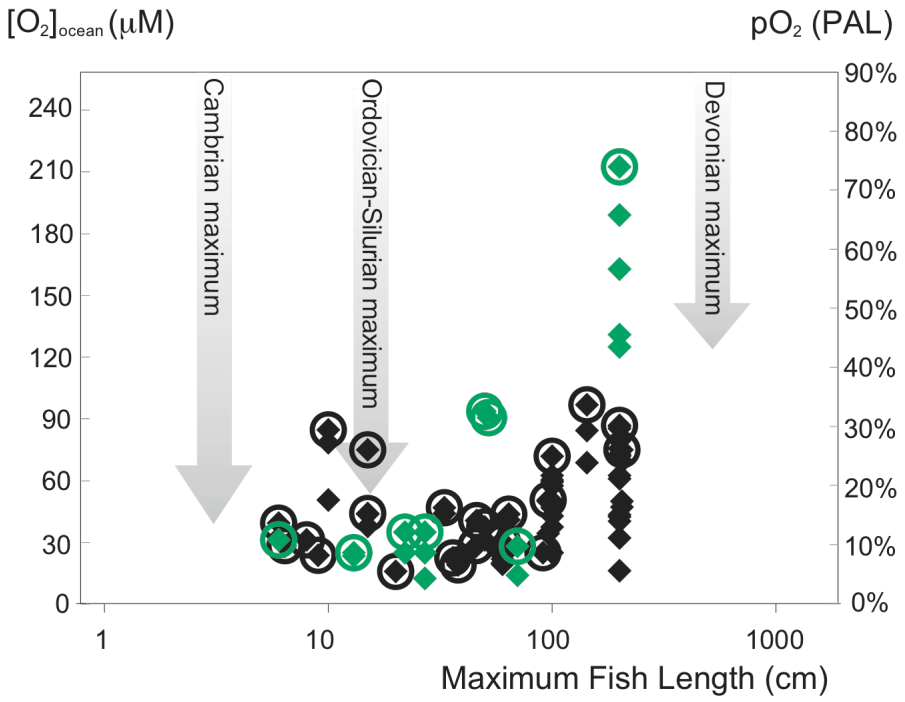

Figure S7: Hypoxia tolerance in modern fish versus maximal length is given in terms of median lethal oxygen concentration LC_{50} (♦) (where 50% of a population is dead) and lowest observable effect concentration (LOEC, ♦) fatal for survival (e.g. growth, metabolism or reproduction). The critical tolerance observed for each species is marked with rings. The maximum fish length in the Paleontological record increases with time (arrows) in concert with increasing minimum O_2 requirement.

Sample descriptions

The material for this δ^{98}Mo compilation consists of 180 black shales (64 samples newly collected and analyzed for this study) from 22 formations (Table S1). Samples were chosen where their iron speciation chemistry suggested deposition beneath a euxinic water column, because such sediments have the potential to record δ^{98}Mo of contemporaneous seawater (32).

Isotope fractionation occurs in mildly euxinic basins where bottom water $H_2S < 11$ mM and/or when [H_2S] is present intermittently (10, 39). Iron speciation data indicate whether sulfide existed in greater abundance than Fe^{2+}, but it cannot differentiate between euxinic basins where Mo isotope fractionation occurred and basins where it did not. Here we describe the stratigraphic units analyzed and discuss evidence that would support local Mo fractionation; i.e. evidence for intermittent changes in local redox. This allows us to deconstruct local fractionation during deposition from global changes in seawater composition, based on a combination of sedimentological, paleontological and geochemical proxies. Robust estimates for δ^{98}Mo composition of seawater is revealed from ten stratigraphic units: the Velkerri Formation, northern Australia (1400 Ma); the Chuar Group, Grand Canyon, USA (742 Ma); the Ara Group, Oman (542 Ma); the Niutitang Formation, Yangtze Platform, China (532 Ma); the Alum Shale, Scania, Sweden (501 Ma); the Upper Hartfell and Birkhill Shales, Dobs Linn, Scotland (442 Ma); the Oatka Creek Formation, New York State (392 Ma); Chattanooga Shale, Tennessee (367 Ma); the Whitby Mudstone Formation, Yorkshire, England (181 Ma); and finally from the modern Black Sea (Table S2). In all other sections described here local fractionation with d^{98}Mo was consistently lower than that predicted by the increase in δ^{98}Mo maxima over time (Figure 1).

Wollogorang Formation, Tawallah Group, drill core Mount Young 2 from northern Australia: ~1730 Ma

The age of this formation is constrained by U-Pb SHRIMP zircon ages of 1729 ± 4 Ma and 1730 ± 3 Ma from tuffaceous green claystone layers from the middle of the black shale unit (40). Samples analyzed for $d^{98}Mo$ represent black shales with high TOC (up to 6 wt %), relatively high Mo concentrations 41-58 ppm (18), and variably high degree of pyritization (DOP) = 0.6-0.9 (18) deposited in a semi-restricted marine intracratonic basin (41) characterized by oxic surface waters with low-sulfate and generally euxinic deep waters (18). Paleomagnetic, petrological and geochemical data, along with geochemical modeling suggests the Wollogorang Formation experienced post-depositional hydrothermal fluid flow, and thus, some samples likely contain a lower $\delta^{98}Mo$ value than seawater. With this possible post-depositional alteration in mind, the best estimate for contemporaneous seawater at 1730 Ma is $\delta^{98}Mo$ = 1.1‰ (18).

Velkerri Formation, Roper Group, drill core from northern Australia: ~1400 Ma

The age of the Velkerri Formation is constrained by new Re-Os dates of 1362 ± 21 Ma and 1417 ± 29 Ma (5) as well as a U-Pb SHRIMP zircon date of 1492 ± 4 Ma from a tuff bed located 700 m beneath the Velkerri Formation (18). Sedimentology (e.g. presence of glauconite), sequence stratigraphy (e.g. six third-order progradational sequences) and geochemical measures (pyrite $\delta^{34}S$) suggest that the Roper Group was deposited in a shelf/ramp setting in an epicratonic basin connected to the global ocean with low sulfate concentrations and a stratified water column (18).

Typical Mo concentrations in the Velkerri Formation fall in the range 11-33 ppm (7). The analyzed samples contain 105-119 ppm Mo, high degree of pyritization, DOP > 0.9, and Fe/Al =1.43-1.85 indicating deposition in a euxinic water column (18). The consistently high $\delta^{98}Mo$ = 0.94-1.13 ‰ (Table S1) is interpreted to reflect seawater at 1400 Ma of 1.1 ‰ (18).

Chuar Group, outcrops from the Grand Canyon, USA: ~742 Ma

The Chuar Group was deposited in an intracratonic rift basin near the equator (42, 43) during break-up of the supercontinent Rodinia(44). Our samples come from the Walcott Member in the uppermost 250 m of the 1400 m thick Chuar Group. This black shale unit is capped by an ash layer hosting zircons with a U-Pb age of 742 ± 6 Ma (44). The presence of the age-diagnostic acritarch *Cerebrosphaera buickii* (45) and diverse vase shaped protist tests (46) suggests that most or all of the group was deposited between about 800 and 742 million years ago.

Sedimentary Fe speciation chemistry suggests that the Chuar basin experienced oxic surface waters but anoxic deep waters, with euxinic conditions prevailing during deposition of the Walcott Member (47). However, the sediments contain low Mo (0.2-12 ppm) and Mo EF (1-20) compared to most Proterozoic black shales(7). Most samples fall around δ^{98}Mo = 1.0‰ which provides the best estimate of contemporaneous Proterozoic seawater.

Tapley Hill Formation and Appila Tillite, drill core sR6 from the Stuart Shelf, Adelaide Rift, Australia: ~645 Ma

The Tapley Hill Formation and Appila Tillite were deposited in the Stuart Shelf basin of the Adelaide Rift Complex, Australia within an epicontinental basin 200 to 300 km wide with apparent open access to the global ocean through the present south basin margin (48). The Appila Tillite was deposited in deep water, and through most of its history, the Tapley Hill Formation was deposited in a basinal setting (48).

The Tindelpina Shale Member at the base of the Tapley Hill Formation has a Re-Os date of 643.0 ± 2.4 Ma(49). Accordingly, the underlying Appilla Tillite is older than this and specifically older than the 635.5±0.5 Ma Marinoan cap carbonate in Namibia (50) that

has previously been correlated with the tillite on the basis of $\delta^{13}C$ and $^{87}Sr/^{86}Sr$ chemostratigraphy (51-53).

Sediments were deposited beneath an anoxic but non-sulfidic water column, where Fe^{2+} was transported in the water column and the ferrous iron supply greatly exceeded the H_2S in the system, preventing complete pyritization (30). Mo concentrations are generally low (~ 1 ppm) with Mo/Al elevated only two-fold over average crustal rocks (Mo EF = 2). Two samples have $\delta^{98}Mo$ = 0.2‰ and 0.8‰, and thus low H_2S may have resulted in isotopic fractionation from seawater Mo.

Dracoisen Formation, outcrops from Spitsbergen: ~625 Ma

The Polarisbreen Group comprises the Elbobreen Formation, overlain by the Wilsonbreen diamictite and the Dracoisen Formation at the top. Samples come from the latter, which has no robust age constraints, but a whole rock Rb-Sr age of 654 ± 23 Ma from the Elbobreen Formation can be regarded as a maximum age (54). The underlying, 150 m thick Wilsonbreen Diamictite is correlated to the Marinoan glaciation (54, 55) based on stratigraphic and geochemical correlations of the underlying Akademikerbreen Group: this implies deposition after 635 Ma of the Dracoisen Formation.

The black shales are enriched in highly reactive iron with negligible pyrite content, indicating deposition in an anoxic and ferruginous water column (30). The same is true for the Elbobreen Formation below the diamictite and the correlative Canyon Formation in East Greenland (30). Samples have considerable Mo abundance and enrichment factors of 6-12 ppm and Mo EF at 5-8, respectively, with a sample at $\delta^{98}Mo$ = 1.1‰ consistent with seawater at or above this value.

Windermere Supergroup, outcrops from the Cariboo Mountains, western Canada: ~608-570 Ma

Samples from the Cariboo Mountains come from the Middle and Upper Kaza Group and the overlying Isaac Formation. The Old Fort Point Formation of the Middle Kaza is a marker unit that is exposed over an area of 35,000 km^2 and has a Re-Os date of 608 ±5 Ma(56). A U-Pb zircon date of 569.6 ± 5.3 Ma is found in volcanic rocks of the Hamill Group that unconformably overlie the Windermere Supergroup, thus constraining the younger age limit.

The Middle and Upper Kaza Group records an extensive submarine sandy turbidite system deposited in a basinal setting; the later deposition of the Isaac Formation took place in a shallower slope setting (57). Bottom water redox conditions, inferred from highly reactive iron, shows that the Middle Kaza Group were deposited under anoxic and ferruginous conditions ($Fe_{HR}/Fe_T < 0.38$) (30); in contrast the Upper Kaza Group was deposited beneath oxic bottom waters. It has been suggested that this redox transition was related to the post-Gaskiers (580-560 Ma) deep-water oxygenation observed in Newfoundland (30) (see below).

Mo abundance is generally low in the Kaza Groups and the Isaac Formation (~ 1 ppm, Mo EF ~ 1), but occasionally reaches ~8 ppm. In samples that contain authigenic Mo enrichments, the bulk isotopic compositions (δ^{98}Mo = -0.4 to +0.2‰) are either reminiscent of dilution with detrital Mo at a δ^{98}Mo similar to average crust (~0‰) or fractionated relative to oceanic input (<0.7‰), or both. Therefore, based on these observations $d^{98}Mo_{sw}$ was ~1.1 ‰ at this time.

Drook and Gaskiers Formations, outcrops from the Avalon Peninsula, Newfoundland, Canada: ~580-565 Ma

Glacial deposits from the Gaskiers Formation are precisely dated, with a U-Pb zircon date of 580 ± 1 Ma from just below the glacial units, and 575 ± 1 Ma from an ash bed in the

overlying Drook Formation. The Drook Formation consists of alternating graded sandstone layers and silty mudstones, with abundant volcanic ash beds deposited in deep waters (below storm wave base), possibly in an arc-related setting with steep subaerial and subaqueous slopes (58, 59). The section famously hosts the oldest Ediacaran fossils, e.g. *Charnia* (60), and recent iron speciation data suggest an abrupt shut off of highly reactive iron supply at the transgressive transition between the Gaskiers glacial deposits and the overlying Drook Formation. This implies changes in local redox conditions from anoxic and ferruginous deep waters to oxic conditions (61). Currently the Drook Formation and/or the Upper Kaza Group in the Windermere Supergroup (see above) represent the oldest evidence for oxic conditions in basinal settings.

Authigenic Mo concentrations in the Gaskiers and Drook Formations are low, with Mo abundances and enrichments of <3 ppm and <3, respectively. However, the ferruginous sediments of the Gaskiers Formation have statistically higher abundances than during the deposition of the Drook Formation, when bottom water contained O_2 (student's t-test, probability = 0.06). The isotopic compositions (δ^{98}Mo = 0.0 ‰ to +0.3 ‰) are similar to the average crust (~0 ‰), which constitutes an important component of bulk Mo. The low bulk d^{98}Mo values are consistent with a low seawater δ^{98}Mo value at 580 Ma and suggest that the authigenic Mo component in the ferruginous samples may have been fractionated locally.

Ara Group, Huqf Supergroup, drill cores MM NW-7 and ALNR-1 from Oman: ~542 Ma

The Ara Group of the uppermost Huqf Supergroup consists of evaporite-carbonate cycles (A0-A6) that record a period of basin restriction in a strongly subsiding foreland trough(62). It was deposited between ~540-550 Ma as constrained by U-Pb zircon dates from ash beds in the A4 carbonate unit, 542 Ma, and basal A0 carbonate unit, 547 Ma(63).

Samples come from drill cores MM NW-7 and ALNR-1 through the Athel silicilite, which represents the deepest part of the South Oman Salt Basin. The samples have high TOC, Mo and Mo EF, consistent with deposition under a sulfidic water column, but Fe speciation data has so far not been reported (64). Reported δ^{98}Mo values (65) show a transition from < 1.3 ‰ with a dramatic oscillation between 0.0 ‰ and 1.5-1.6‰ and subsequent fall to 1.1 - 1.3 ‰, which reflects the best estimate of seawater at that time. The highest value reflects substantial Mo removal from the ocean that occurred with fractionation, e.g. a large oxic sink relative to sulfidic Mo removal.

Niutitang Formation, outcrops from the Yangtze Platform, China: ~532 Ma

The Niutitang Formation consists of black shales resting unconformably on the ~700 m thick carbonate-rich Denying Formation(66). A polymetallic sulfide marker bed occurs a few meters above the base of the Niutitang Formation, displaying unusual metal enrichments such as 3-9 wt% Mo. The Formation was first correlated with the Ara Group based on δ^{13}C chemostratigraphy and a Re-Os date of 541 ± 16 Ma from the metal rich layer(67). However, a new SHRIMP U-Pb zircon date of 532.3 ± 0.7 Ma (within the error margins of the Re-Os age) from a volcanic ash bed in the lowermost black shale sequence in the Guizhou Province accurately constrains the age of the Niutitang Formation (66) indicating deposition slightly later than the Ara Group.

Apart from the polymetallic sulfide marker bed, the black shales have similar Mo, Mo EF, and TOC to the other Proterozoic and some of the Phanerozoic shales in our sample set (64). δ^{98}Mo values are around 1.1-1.3 ‰ with a peculiar peak at 1.9‰ (one sample) followed stratigraphically by low values of δ^{98}Mo of 0.5-0.8 ‰ and a return to 1.1 ‰ (65). Mo/TOC show large variations, at 7-41 ppm/wt%, decoupled from δ^{98}Mo, implying that changes in seawater composition alone are insufficient to explain the data. The presence of highly metalliferous sediments with 3-7 wt% Mo may indicate that syndepositional hydrothermal fluids dominates the Mo budget of this basin (68, 69), although it has been suggested that all Mo in the ore horizon came from seawater (33). Additionally, we cannot eliminate the possibility that fractionation took place during

deposition, especially during the interval of low δ^{98}Mo. In any case, the most positive δ^{98}Mo values of 1.1-1.3 ‰ probably reflect a time when seawater re-established dominance in the local Mo budget shortly after 532 Ma.

Yu'anshan Shale, Ma'Fang drill core from Chengjiang, Yangtze platform, China: 521-517 Ma

The Yu'anshan Shale is one of four members belonging to the Helinpu (formerly Qiongzhusi) Formation (70) (for division see (71)). Our core samples, from the Ma'fang core drilled in June 2008, come from the second member, which is carbonaceous black shale characterized by high TOC, pyrite, and dolomite lenses. This member is overlain by the fossiliferous Maotianshan Shale Member, a claystone interbedded with discontinuous siltstones (72) that contains the Chengjiang Lagerstätten (71-73). The Yu'anshan Shale has been interpreted to represent a single shallowing-upward sequence, but specific environments and modes of deposition are still under discussion (71, 74). It has been suggested that deposition took place in a tropical sea, bordered on all sides by landmasses (75), but sedimentological evidence for tidal structures (74) requires a significant connection to the open ocean. Our samples are interpreted to represent a deep-water environment in a semi-restricted basin.

Absolute dates have not been established for the Yu'anshan Shale, but biostratigraphic correlation of small shelly fossils, trilobites and acritarchs suggests it was deposited during the late Atdabanian Stage, ca. 521-517 Ma (71, 74, 76-79), with the first appearance of trilobites occurring at its base (73, 80).

According to our Fe speciation data, the Yu'anshan Shale records euxinic deposition (Fe_{HR}/Fe_{TOT} = 0.48±0.06, Fe_{PY}/Fe_{HR} = 0.86±0.02). The samples have ~2 wt % organic carbon, moderately high Mo concentrations and enrichments (8-19 ppm; Mo EF = 5-12) and isotope composition tightly clustered in two groups at 1.1 ‰ (43.8-45.6 m, depth)

and 0.6‰ (47.6-48.5 m, depth). We interpret these values to reflect fractionation with seawater δ^{98}Mo of >1.1 ‰.

Burgess Shale Formation, outcrops from British Colombia, Canada: ~505 Ma

The Walcott Quarry Shale Member of the Burgess Shale Formation contains finely laminated, calcareous, silty and graphitic mudstones (81) deposited in a marine setting with an exceptionally well-preserved fossil fauna (82). Our samples come from shales 13-40 cm below the original floor of the "Phyllopod Bed" (the Marella Layer), as it was named by its discoverer, C. D. Walcott in 1912.

The exceptional fossil preservation is often attributed to anoxic bottom waters. However, this conclusion is challenged by the lack of trace metal enrichments (Mo, U/Th, V/Cr, Ni/Co, V/Ni, V/Sc) in the Burgess Shale Formation (83). Our analyses support this finding with low Mo and TOC (TOC = 0.2-0.3 wt %; Mo <2 ppm) that we associate with a general absence of sulfide in the bottom waters. However, some samples are enriched in highly reactive iron (Fe_{HR}/Fe_T = 0.5-0.6), implying Fe^{2+} transport and deposition in anoxic waters. Two of the samples display low Fe_{HR}/Fe_T values and substantial pyrite fractions (Fe_P/Fe_{HR} = 0.25-0.48) associated with δ^{98}Mo = 0.2 ‰. The heaviest sample deposited under an anoxic, non-sulfidic water column is significantly heavier than detrital inputs, but consistent with seawater at δ^{98}Mo > 0.9 ‰.

Cambrian-Silurian shales drill core samples from Baltica: 505-430 Ma

The Baltic samples (Alum-, Almelund-, and Rastrites shale Formations) derive from a condensed Lower Paleozoic succession, deposited in a sediment starved epicontinental basin (84). The sampled Cambro-Ordovician units represent outer shelf shales and mudstones that accumulated at average rates of ~2-5 mm/1000 yrs (85, 86). The Silurian shales, representing a distal foreland basin setting, are less condensed. The epicontinental sea is generally assumed to have been in open access with the global ocean, but it is possible that uplift of the craton margin, associated with initial subduction in the Iapetus

Ocean, to some extend restricted the water exchange during the Mid Cambrian-Tremadocian. This caused stratification of the water column and low oxygen (mostly anoxic?) conditions at the sea floor. The presence of an abundant albeit low-diverse trilobite fauna, including many species that are found elsewhere (87), in the Alum Shale Formation indicates that marine conditions still prevailed.

The investigated units are highly fossiliferous and well-dated biostratigraphically. Deposition ages are derived from the biozones (88) and interpolated linearly by depth in the drill cores as in ref. (86) (Table S1).

Alum Shale Formation, Scania, Sweden: 505-485 Ma

Drill cores: Andrarum-3, SE Scania, Albjära-1, W. Scania, Gislövhammar-2, SE Scania.

Samples come from three drill cores in Scania, Sweden, straddling a 20 million year interval from the late Mid Cambrian to the mid Tremadocian. The Andrarum-3 drill core covers the uppermost Middle Cambrian to lower Furongian (*A. pisiformis* and *Olenus* superzones). The mentioned biozones are separated by a global oceanic anoxic event referred to as the 'SPICE' $\delta^{13}C$ excursion(89). Drill core samples from Albjära-1, W. Scania and Gislövhammar-2, SE Scania, cover the middle Tremadocian (*A. tenellus* and *Kiaerograptus* zones). Locations of drill cores are shown in Fig. 1 of ref. (86).

The Alum Shale Formation comprises extraordinarily organic-rich black shales – up to 25 % TOC - with high pyrite content (85, 86). The shales are laminated with only rare traces of bioturbation, suggests the imposition of anoxia within the sediments. It contains a low-diverse but highly abundant fossil fauna, dominated by trilobites and brachiopods (87), implying at least intermittent presence of oxygen (90). The occurrence of a benthic fauna is at odds with the geochemical data, suggestive of anoxic and euxinic conditions (see below). The fossiliferous interludes possibly reflect short-lived oxygenation events. Graptolites are common in the Ordovician interval (91), but these pelagic organisms only have indirect bearing on the chemical conditions at the sea floor; their preservation would

be enhanced under mostly anoxic conditions.

The mid-Cambrian Furongian samples display high Fe_{HR}/Fe_T = 0.6-1.0 and high Fe_P/Fe_{HR} > 0.9 and thus evidence for Fe^{2+} delivery to an anoxic and sulfidic basin. This interpretation is supported by high Mo concentrations (25-125 ppm) and disseminated 1-10 mm pyrite framboids (*46*). Significant variability in δ^{98}Mo = 1.0-1.4‰ around the oceanic anoxic event (SPICE) indicates a response to global redox changes in a setting, where local redox conditions show little, if any, variation. At all times euxinic samples would have δ^{98}Mo up to 1.4‰ at ~500 Ma.

The Ordovician samples also indicate anoxic and euxinic deposition, Fe_{HR}/Fe_T = 0.7-0.9, and Fe_P/Fe_{HR} = 0.64-0.74, but again the presence of benthic brachiopods require at least brief periods with oxic seafloor. Mo concentrations and isotopic composition vary greatly by Mo EF = 4-17; 34-75 and δ^{98}Mo = 0.28-0.54; 0.67-1.12‰ in Albjära-1 and Gislövhammar-2, respectively. Besides, the sub-riverine ä^{98}Mo values in Gislövhammar-2 imply that considerable isotope fractionation occurred during deposition. In combination, the high variability and low δ^{98}Mo values together with presence of benthic brachiopods indicate short-lived oxygenation events, while excess highly reactive iron reflect overall anoxic conditions in the basin.

Almelund Shale, Scania,Sweden, Middle Ordovician (Darriwilian) 465-462 Ma
Drill core: Albjära-1, W. Scania,

The Almelund Shale is black, but contains significantly less organic matter than the older Alum Shale (c. 2 wt% TOC). It contains a rich graptolite fauna, often associated with small inarticulate brachiopods (92, 93). . The investigated samples derived from the *H. lentus*, *P. distichus* and *H. teretiusculus* zones Local bottom waters were anoxic, Fe_{HR}/Fe_T = 0.36-0.90 and sulfidic Fe_P/Fe_{HR} = 0.71-0.73. Both Mo enrichments and δ^{98}Mo are low, at Mo EF = 3 and 0.66-0.93‰. As for the Ordovician Alum Shale, benthic brachiopods are present in these core samples indicating at least intermittent oxic conditions. The Fe speciation data is taken to reflect overall euxinic deposition with brief

oxic periods allowing transient invasion by an opportunistic benthic fauna. The isotope composition of these shales are consistent with a $\delta^{98}Mo_{SW}$ value at >0.9‰.

Rastrites Shale, Scania-Bornholm, Upper Ordovician-Lower Silurian (Hirnantian-Telychian) 444-430 Ma

Drill cores: Billegrav-1, Bornholm; Lönstorp-1, W. Scania

The samples analyzed for Mo in Billegrav-1 and Lönstorp-1 come from the Ordovician-Silurian boundary interval (*persculptus* and *ascensus* graptolite zones (94, 95). Also these shales are grey to blackish, and contain < 3 wt% TOC (86). The fauna is dominated by graptolites with subordinate presence of cephalopods (95). The geochemical data suggest that deposition took place under a largely euxinic water column (Fe_{HR}/Fe_T = 0.42-0.52, Fe_P/Fe_{HR} = 0.72-0.78). The elevated Mo abundance (~7-18 ppm) and Mo EF = 3-8 provide supporting evidence for the presence of H_2S, but the low $d^{98}Mo$ value 0.58‰ (one sample) is ~0.8‰ lighter than the heaviest contemporaneous euxinic shales (Dobs Linn). The presence of a benthic fossil fauna in the samples implies mildly sulfidic or intermittent oxic conditions that allow isotope fractionation to occur. Younger Silurian samples from the Lönstorp core (*convolutes, guerichae, griestoniensis* and *spiralis* graptolite zones) display Fe_{HR}/Fe_T < 0.38 indicative of oxic deposition, where Mo is not necessarily preserved.

Upper Hartfell and Birkhill Shales, outcrops from Dob's Linn, Southern Uplands, Scotland: ~444 Ma

Dob's Linn in southern Scotland is the global stratotype (GSSP) for the base of the Silurian (443.7±1.5 Ma) (96, 97), and records a deep-water sequence of graptolitic shales and mudstones from a tropical, continental margin setting facing the Iapetus Ocean (98). The section exposes the Upper Hartfell and Birkhill Shales (belonging to the Upper Ordovician Katian – Hirnantian stages), and straddles two Late Ordovician extinction events. The first extinction is associated with cooling at the onset of the Hirnantian glacial maximum (99), which also saw regression, and persisted for the duration of the

extraordinarius graptolite Zone. The short-lived glaciation ended with transgression during the latest Ordovician *persculptus* Zone, resulting in deposition of the black, laminated Birkhill Shales, which record the second extinction and are the focus of this study. This regressive-transgressive sea level history is seen to be a eustatic signal (100), suggesting a connection with the global oceans. This is confirmed by the presence of a ubiquitous and biostratigraphically important graptolite fauna (hence the choice of the section as the GSSP).

Samples are taken from the black, laminated Birkhill Shales, which are enriched in highly reactive iron and contain moderately high Fe_P/Fe_{HR} = 0.37-0.73 indicating deposition in an anoxic and mostly euxinic water column. This conclusion is corroborated by the presence of high Mo enrichments (Mo EF ~10) requiring the presence of H_2S. The moderately high pyrite content and sudden depletions of Mo may suggest cyclic redox changes associated with chemocline fluctuations. δ^{98}Mo correlates with Mo enrichments with dramatic variation from -0.2 and 1.44 ‰. These systematic variations imply that isotope fractionation took place during deposition of the Mo depleted sediments, thus we interpret early Silurian seawater as the highest recorded value, δ^{98}Mo = 1.4-1.5‰.

Soom Shale, drill core from Clanwillian, South Africa: ~453-443 Ma

The Soom Shale samples (n = 3) are from core material, drilled close to the Keurbos quarry in Clanwillian, South Africa. They are fine silts and mudstones, laminated on a millimeter scale and deposited in the late Katian or early Hirnantian (Late Ordovician). The depositional setting of the basinal shales of the Soom has been variously interpreted as glacio-lacustrine to shallow marine (101). No structures produced by storm waves have been identified in the Soom Shale, indicating water column depths below 100 m (102), but not much deeper as it overlies the tillites of the Pakhuis Formation, and itself is overlain by the shallow marine Disa Siltstone Member. Alternatively, storm induced structures may have been prohibited by periodic ice-sheet cover indicated by the presence of dropstones in the basinal shales (103).

Redox conditions are difficult to assess, because there is no enrichment of highly reactive iron (Fe_{HR}/Fe_{TOT} = 0.31±0.03) in our samples, but an extended study shows the deposition environment was indeed anoxic Fe_{HR}/Fe_{TOT} = 0.40 and ferruginous Fe_{PY}/Fe_{HR} = 0.29±0.01(104) with at least some sulfide in the pore fluids consistent with the high Mo concentrations (~30 ppm). The organic content is low (~0.5 wt %) which may mean that sedimentary sulfate reduction was TOC limited in an anoxic water column with incomplete pyritization of reactive Fe. Under these conditions, we do not expect quantitative Mo removal, so δ^{98}Mo of contemporaneous seawater must have been >1.29 ‰ during the Late Ordovician.

Oatka Creek and Geneseo Formations, and Chattanooga and New Albany Shales, drill cores and outcrops from eastern USA: ~392-360 Ma

Four shale formations from the Illinois and Appalachian Basins of the USA have been included in this study. These sediments were deposited in an intracratonic marine basin at southern tropical latitudes (98). The formations are described below in chronological order: Oatka Creek Formation, Geneseo Formation, Chattanooga Shale and New Albany Shale. All age determinations are based on conodont and goniatite biostratigraphic correlations(105) with interpolated absolute ages based on average stage ages from ref. (88).

Oatka Creek Formation, Akzo drill core #9455: ~392 Ma

The Oatka Creek Formation contains the upper *kockelianus* and lower *ensensis* conodont biozones(106) and was therefore deposited during the Late Eifelian, between 390.1 ± 2.5 Ma(107) and 391.8 ± 2.7 Ma based on the ICS model (88). It consists of finely laminated organic-rich black shales with a high pyrite content, deposited in the deeper part of the Appalachian Basin where bottom waters were mostly anoxic and sulfidic (32, 108, 109).

Accordingly, the Oatka Creek Formation displays significant Mo enrichments (400 ppm Mo; Mo EF 100-300) and high Mo/TOC = 20 ppm/wt %, similar to modern euxinic sediments. Seawater δ^{98}Mo is most likely found in samples with the highest pyrite content, and samples with DOP = $Fe_{Pyrite}/Fe_{HCl} > 0.9$, display δ^{98}Mo = 1.7-2.0 ‰ (32). It is therefore likely that Middle Devonian oceans were similar δ^{98}Mo values, or perhaps -0.3 ‰ lighter than modern seawater.

Geneseo Formation, Akzo drill core #9455: ~383 Ma

The Geneseo Formation was deposited ~5 Myr after the Oatka Creek Formation in the Appalachian Basin. It contains the *disparilis* conodont biozone of the Late Givetian (32, 105, 108, 109). The Geneseo Formation has a lower degree of pyritization (DOP < 0.4), modest Mo enrichments (Mo EF < 20; 30 ppm Mo), and significantly lower δ^{98}Mo values (0.9-1.3‰), but still higher than older non-euxinic sediments suggesting Mo removal in sulfidic pore fluids that may occasionally have breached into the water column (32). No Fe speciation data has been published, so we cannot exclude permanently anoxic or mildly euxinic conditions (e.g. $[H_2S] < 11$ mM). We note that δ^{98}Mo in the Geneseo Formation is 0.7-1.1‰ lighter than other Middle Devonian shales, consistent with the observed fractionation in modern oxic sediments with sulfidic pore waters and with Late Devonian seawater at δ^{98}Mo = 2.0 ‰.

Chattanooga Shale, outcrops in Tennessee: ~375-360 Ma

Samples from the Clegg Creek Member of the New Albany Shale (n = 2), were deposited in the Illinois Basin, ~300 km north of the site of the contemporaneously deposited Chattanooga Shales. Basinal conditions at the two sites were similar and will be discussed together below.

The Upper Gassaway Member of the Chattanooga Shale, Tennessee, covers four Famennian conodont biozones (*trachytera, postera, expansa, praesulcata*) between 374.5 and 359.2Ma (88, 110). Outcrops are weathered and samples were taken after cleaning

off oxidation rinds on fractures (thin sections show pristine pyrite framboids beyond 1 mm from the fracture surface (Jürgen Schieber, pers. communication)). The redox state during deposition is debated, with biomarker evidence for photic zone euxinia through the time equivalent shales from the Illinois Basin (111), but with fossil evidence for benthic oxia provided by the presence of agglutinated benthic foraminifera (112). However, the shales are finely laminated without signs of severe bioturbation suggesting some degree of bottom water oxygen depletion (113, 114). Our iron speciation data point to a euxinic signal for both sample sites, with $Fe_{HR}/Fe_T = 0.66 \pm 0.06$ and $Fe_{PY}/Fe_{HR} = 0.73 \pm 0.07$. This is corroborated by a high TOC of ~9 wt % and strong Mo enrichment, 100 times crustal average, only observed in modern euxinic environments. δ^{98}Mo values are 1.45 - 1.66‰ and 1.73 - 1.93‰ in the Chattanooga Shale and the Clegg Creek Member of the New Albany Shale, respectively. We hold that deposition was dominated by overall euxinic conditions, with d^{98}Mo of seawater at ~ 2 ‰, captured during periods with minimal fractionation in the sediments.

Whitby Mudstone Formation, outcrops in Yorkshire, England: ~183 Ma

The Whitby Mudstone Formation consists of mudstones deposited in a large epicontinental seaway that covered much of Europe during the Jurassic (115, 116). The Formation has been subdivided stratigraphically into three members: in ascending order, the Grey Shale, Mulgrave Shale, and Alum Shale (117). A portion of the upper Grey Shale and the basal, most organic-rich portion of the Mulgrave Shale have been linked to the Toarcian Oceanic Anoxic Event (T-OAE) (118, 119). Sedimentologically, the Whitby Mudstone Formation consists predominantly of mudstones with prominent and distinctive horizons which bear carbonate concretions (120, 121). In the Mulgrave Shale these mudstones are predominantly laminated, organic and pyrite-rich (122-124). Geochemical and sedimentological indicators (DOP, DOP_T, organic biomarkers and pyrite framboid size distributions) suggest that at least some of the upper Grey Shale, and most of the Mulgrave Shale, were deposited under anoxic and sulfidic conditions (124-127). However, frequent beds of inoceramid bivalves indicate periodic benthic ventilation (122). The benthic habitation and ventilation events appear to have been geologically

brief, based on the large-scale preservation of lamination and high organic content of the sediments (124).

Mo concentrations and isotope data have been published (128) from the upper Grey Shale through lowest Alum Shale. Both parameters show a considerable range in values: 0.39 to 42.97 ppm and -0.46 ‰ to 2.14 ‰. The low values found in the basal Mulgrave Shale have been attributed to depletion of the molybdenum reservoir during the T-OAE (128), an assertion that was challenged (127) citing local restriction and draw down. With the possible complications in the interpretation of the Mo isotope data in mind, we take the best estimate of Jurassic seawater as 2.14‰.

Compilation of Mo/TOC in euxinic black shales

The compilation constitutes of new samples in Table S1 and published data listed in Table S4.

Table S6: List of data sources and age assignments for Mo/TOC compilation (Figure 3c).

Location	Unit	Series/Stage	Age	Ref.
Black Sea	Sta9 and Sta14	Modern	0	117
Cariaco, Basin, Venezuela	ODP Site 1002	Modern	0	118
California, USA	Monterey.	Miocene	20	119
Colombia/Venezuela	La Luna	Cenomanian-Campanian	77.1	35, 36
Mediterranean Sea	ODP Sites 975, 974, 964, 969, and 967	Cenomanian-Albian	93.5-105	120
Queensland, Australia	Julia Creek, Toolebuc	Cretaceous	100	121
Yorkshire, UK	Kimmeridge Clay	Kimmeridgian	153.3	122
Germany	Posidonia Shale	L. Toarcian	183	123
Yorkshire, UK	Whitby Mudstone	Toarcian	183	19,116
W. Wyoming, USA	Phosphoria Basin	Roadian-Wordian	268	124
SE Idaho, USA	Phosphoria Basin	Roadian-Wordian	270	125
Iowa, Oklahoma, USA	Hushpuckney, Tacket shale	Missourian	306	126
Kansas, NE	Stark Shale	Missourian	306	127
S. Iowa, N. Missouri, SE Kansas, NE Oklahoma	Excello Shale	Mid-Pennsylvanian	306-308	128
Alberta, Canada	Exshaw	Famennian-Tournaisian	359.2	129
Kentucky, USA	Sunbury, Bedford, Cleveland shale. Three-Lick, Huron	Late Famennian - Early Tournaisian	355.7-374	130

British Columbia, Canada	Upper Besa River	Famennian-Tournaisian	355	131
British Columbia, Canada	Lower Besa River, Muskwa	Givetian-L/ Frasnian	385	131
British Columbia, Canada	Golata	Visean-Serphukovian	326	131
British Columbia, Canada	Fort Simpson	Frasnian	380	131
Kentucky, Ohio, Tennessee, USA	Ohio and Chattanooga shale	U. Devonian	374	132
Kentucky, USA	Huron, Cleveland Mbr of New Albany Shale	E. Famennian	374	133
Illinois, USA	Grassy Creek	U. Devonian	374.5	134
New York, USA	Oatca Creek	Eifelian/Givetian	391.8	95
Bardzkie Mtns, SW Poland	Zdanow	Pridoli-Lochkovian	416	135
Scania, Sweden	Alum shale	Furongian	501	136
Yangtze Platform, China	Niutitang	L. Cambrian	532	58
Central Hunan, China	Dongping, Yanxi, Taojiang, Ningxiang	L. Cambrian	521	137
Oman	Ara Group	Ediacaran-Cambrian	542	58
Yangtze Platform, China	Datangpo	Cryogenian	663	7
Yangtze Platform, China	Doushantuo	Ediacaran	556-635	

References

1. Shimmield G & Price N (1986) The behaviour of molybdenum and manganese during early sediment diagenesisóoffshore Baja California, Mexico. *Mar. Chem* 19:261-280.
2. Bertine K & Turekian K (1973) Molybdenum in marine deposits. *Geochim. Cosmochim. Acta* 37:1415-1434.
3. Crusius J, Calvert S, Pedersen T, & Sage D (1996) Rhenium and molybdenum enrichments in sediments as indicators of oxic, suboxic and sulfidic conditions of deposition. (Translated from English) *Earth Planet. Sci. Lett.* 145(1-4):65-78 (in English).
4. Morford J, Emerson S, Breckel E, & Kim S (2005) Diagenesis of oxyanions (V, U, Re, and Mo) in pore waters and sediments from a continental margin. *Geochimica Et Cosmochimica Acta* 69(21):5021-5032.
5. Wasylenki LE, Weeks CL, Spiro TG, Bargar JR, & Anbar AD (2009) How Mo isotopes fractionate during adsorption to Mn and Fe oxyhydroxides. (Pergamon-Elsevier Science Ltd), pp A1419-A1419.
6. Erickson BE & Helz GR (2000) Molybdenum(VI) speciation in sulfidic waters: Stability and lability of thiomolybdates. *Geochim. Cosmochim. Acta* 64(7):1149-1158.
7. Scott C*, et al.* (2008) Tracing the stepwise oxygenation of the Proterozoic ocean. *Nature* 452(7186):456-459.
8. Zheng Y, Anderson RF, van Geen A, & Kuwabara J (2000) Authigenic molybdenum formation in marine sediments: A link to pore water sulfide in the Santa Barbara Basin. (Translated from English) *Geochim. Cosmochim. Acta* 64(24):4165-4178 (in English).
9. Brucker RLP, McManus J, Severmann S, & Berelson WM (2009) Molybdenum behavior during early diagenesis: Insights from Mo isotopes. (Translated from English) *Geochemistry Geophysics Geosystems* 10:25 (in English).
10. Neubert N, Nagler TF, & Bottcher ME (2008) Sulfidity controls molybdenum isotope fractionation into euxinic sediments: Evidence from the modern Black Sea. (Translated from English) *Geology* 36(10):775-778 (in English).
11. Arnold GL, Anbar AD, Barling J, & Lyons TW (2004) Molybdenum isotope evidence for widespread anoxia in mid-proterozoic oceans. *Science* 304(5667):87-90.
12. Siebert C, Nagler TF, von Blanckenburg F, & Kramers JD (2003) Molybdenum isotope records as a potential new proxy for paleoceanography. *Earth Plan. Sci. Lett.* 211(1-2):159-171.
13. Siebert C, McManus J, Bice A, Poulson R, & Berelson WM (2006) Molybdenum isotope signatures in continental margin marine sediments. *Earth Planet. Sci. Lett.* 241(3-4):723-733.
14. Reitz A, Wille M, Nagler TF, & de Lange GJ (2007) Atypical Mo isotope signatures in eastern Mediterranean sediments. *Chemical Geology* 245:1-8.
15. Poulson RL, Siebert C, McManus J, & Berelson WM (2006) Authigenic molybdenum isotope signatures in marine sediments. *Geology* 34(8):617-620.
16. Wasylenki LE, Rolfe BA, Weeks CL, Spiro TG, & Anbar AD (2008) Experimental investigation of the effects of temperature and ionic strength on Mo

isotope fractionation during adsorption to manganese oxides. *Geochim. Cosmochim. Acta* 72(24):5997-6005.
17. Barling J & Anbar AD (2004) Molybdenum isotope fractionation during adsorption by manganese oxides. *Earth Planet. Sci. Lett.* 217(3-4):315-329.
18. Kendall B, Creaser RA, Gordon GW, & Anbar AD (2009) Re-Os and Mo isotope systematics of black shales from the Middle Proterozoic Velkerri and Wollogorang Formations, McArthur Basin, northern Australia. *Geochim. Cosmochim. Acta* 73(9):2534-2558.
19. McArthur J, Algeo T, van de Schootbrugge B, Li Q, & Howarth R (2008) Basinal restriction, black shales, Re-Os dating, and the Early Toarcian (Jurassic) oceanic anoxic event. *Paleoceanography* 23(4).
20. Peneva E, Stanev E, Belokopytov V, & Le Traon PY (2001) Water transport in the Bosphorus Straits estimated from hydro-meteorological and altimeter data: seasonal to decadal variability. (Translated from English) *Journal of Marine Systems* 31(1-3):21-33 (in English).
21. Canfield DE & Teske A (1996) Late Proterozoic rise in atmospheric oxygen concentration inferred from phylogenetic and sulphur-isotope studies. (Translated from English) *Nature* 382(6587):127-132 (in English).
22. Wheat C, Mottl M, & Rudnicki M (2002) Trace element and REE composition of a low-temperature ridge-flank hydrothermal spring. *Geochim. Cosmochim. Acta* 66(21):3693-3705.
23. Archer C & Vance D (2008) The isotopic signature of the global riverine molybdenum flux and anoxia in the ancient oceans. (Translated from English) *Nat. Geosci.* 1(9):597-600 (in English).
24. McManus J, Nagler TF, Siebert C, Wheat CG, & Hammond DE (2002) Oceanic molybdenum isotope fractionation: Diagenesis and hydrothermal ridge-flank alteration. *Geochemistry Geophysics Geosystems* 3.
25. Hannah JL, Stein HJ, Wieser ME, de Laeter JR, & Varner MD (2007) Molybdenum isotope variations in molybdenite: Vapor transport and Rayleigh fractionation of Mo. (Translated from English) *Geology* 35(8):703-706 (in English).
26. Malinovsky D, Hammarlund D, Ilyashuk B, Martinsson O, & Gelting J (2007) Variations in the isotopic composition of molybdenum in freshwater lake systems. (Translated from English) *Chemical Geology* 236(3-4):181-198 (in English).
27. Malinovsky D, Rodushkin I, Baxter D, Ingri J, & Öhlander B (2005) Molybdenum isotope ratio measurements on geological samples by MC-ICPMS. *Int. J. Mass Spectrom.* 245(1-3):94-107.
28. Goldberg T, Archer C, Vance D, & Poulton SW (2009) Mo isotope fractionation during adsorption to Fe (oxyhydr)oxides. *Geochim. Cosmochim. Acta* 73(21):6502-6516.
29. Raiswell R & Canfield DE (1998) Sources of iron for pyrite formation in marine sediments. (Translated from English) *Am. J. Sci.* 298(3):219-245 (in English).
30. Canfield DE*, et al.* (2008) Ferruginous conditions dominated later neoproterozoic deep-water chemistry. (Translated from English) *Science* 321(5891):949-952 (in English).

31. Reinhard C, Raiswell R, Scott C, Anbar A, & Lyons T (2009) A late Archean sulfidic sea stimulated by early oxidative weathering of the continents. *Science* 326(5953):713.
32. Gordon G*, et al.* (2009) When do black shales tell molybdenum isotope tales? *Geology* 37(6):535.
33. Gray J, Wu R, & Or Y (2002) Effects of hypoxia and organic enrichment on the coastal marine environment. *Mar. Ecol. Prog. Ser* 238:249-279.
34. Vaquer-Sunyer R & Duarte C (2008) Thresholds of hypoxia for marine biodiversity. *Proc. Nat. Acad. Sci.* 105(40):15452.
35. Clarke A & Johnston N (1999) Scaling of metabolic rate with body mass and temperature in teleost fish. *Journal of Animal Ecology* 68(5):893-905.
36. Brett J (1972) The metabolic demand for oxygen in fish, particularly salmonids, and a comparison with other vertebrates. *Respiration physiology* 14(1-2):151-170.
37. Young GC (2009) Large Brachythoracid Arthrodires (Placoderm fishes) from the Early Devonian of Wee Jasper, New South Wales, Australia, with a discussion of basal Brachythoracid Characters. *Journal of Vertebrate Paleontology* 24(1):1-17.
38. Payne J*, et al.* (2009) Two-phase increase in the maximum size of life over 3.5 billion years reflects biological innovation and environmental opportunity. *Proc. Nat. Acad. Sci.* 106(1):24.
39. Dahl TW*, et al.* (2010) The behavior of molybdenum and its isotopes across the chemocline and in the sediments of sulfidic Lake Cadagno, Switzerland. (Translated from English) *Geochim. Cosmochim. Acta* 74(1):144-163 (in English).
40. Page R, Jackson M, & Krassay A (2000) Constraining sequence stratigraphy in north Australian basins: SHRIMP U-Pb zircon geochronology between Mt Isa and McArthur River*. *Australian Journal of Earth Sciences* 47(3):431-459.
41. Shen Y, Canfield D, & Knoll A (2002) Middle Proterozoic ocean chemistry: evidence from the McArthur Basin, northern Australia. *Am. J. Sci.* 302(2):81-109.
42. Timmons JM, Karlstrom KE, Dehler CM, Geissman JW, & Heizler MT (2001) Proterozoic multistage (ca. 1.1 and 0.8 Ga) extension recorded in the Grand Canyon Supergroup and establishment of northwest- and north-trending tectonic grains in the southwestern United States. (Translated from English) *Geol. Soc. Am. Bull.* 113(2):163-180 (in English).
43. Weil AB, Geissman JW, & Van der Voo R (2004) Paleomagnetism of the Neoproterozoic Chuar Group, Grand Canyon Supergroup, Arizona: implications for Laurentia's Neoproterozoic APWP and Rodinia break-up. (Translated from English) *Precambrian Res.* 129(1-2):71-92 (in English).
44. Karlstrom KE*, et al.* (2000) Chuar Group of the Grand Canyon: Record of breakup of Rodinia, associated change in the global carbon cycle, and ecosystem expansion by 740 Ma. (Translated from English) *Geology* 28(7):619-622 (in English).
45. Nagy RM, Porter SM, Dehler CM, & Shen Y (2009) Biotic turnover driven by eutrophication before the Sturtian low-latitude glaciation. (Translated from English) *Nat. Geosci.* 2(6):414-417 (in English).

46. Porter S, Meisterfeld R, & Knoll A (2003) Vase-shaped microfossils from the Neoproterozoic Chuar Group, Grand Canyon: a classification guided by modern testate amoebae. *J. Paleontol.* 77(3):409.
47. Johnston DT*, et al.* (2010) An emerging picture of Neoproterozoic ocean chemistry: Insight from the Chuar Group, Grand Canyon, USA. *Earth Planet. Sci. Lett.* 290:64-73.
48. Coats RP, Forbes BG, & Preiss WV (1987) The Adelaide Geosyncline: Late Proterozoic Stratigraphy, Sedimentation, Palaeontology and Tectonics. eds The Hon RG & Payne MP (Ministry of Mines and Energy).
49. Kendall B, Creaser RA, & Selby D (2006) Re-Os geochronology of postglacial black shales in Australia: Constraints on the timing of "Sturtian" glaciation. (Translated from English) *Geology* 34(9):729-732 (in English).
50. Hoffmann KH, Condon DJ, Bowring SA, & Crowley JL (2004) U-Pb zircon date from the Neoproterozoic Ghaub Formation, Namibia: Constraints on Marinoan glaciation. (Translated from English) *Geology* 32(9):817-820 (in English).
51. Kaufman AJ, Knoll AH, & Narbonne GM (1997) Isotopes, ice ages, and terminal Proterozoic earth history. (Translated from English) *Proc. Natl. Acad. Sci. U. S. A.* 94(13):6600-6605 (in English).
52. Kaufman AJ & Knoll AH (1995) Neoproterozoic Variations in the C-isotopic Composition of Seawater - Stratigraphic and Biogeochemical Implications. (Translated from English) *Precambrian Res.* 73(1-4):27-49 (in English).
53. Halverson GP, Dudas FO, Maloof AC, & Bowring SA (2007) Evolution of the Sr-87/Sr-86 composition of Neoproterozoic seawater. (Translated from English) *Palaeogeography Palaeoclimatology Palaeoecology* 256(3-4):103-129 (in English).
54. Fairchild IJ & Hambrey MJ (1995) Vendian Basin Evolution in East Greenland and NE Svalbard. (Translated from English) *Precambrian Res.* 73(1-4):217-233 (in English).
55. Halverson G, Maloof A, Schrag D, Dudas FO, & Hurtgen M (2007) Stratigraphy and geochemistry of a ca. 800 Ma negative carbon isotope interval in northeastern Svalbard. *Chem. Geol.* 237(1-2):5-27.
56. Kendall B, Creaser R, Ross G, & Selby D (2004) Constraints on the timing of Marinoan ìSnowball Earthî glaciation by 187Reñ187Os dating of a Neoproterozoic, post-glacial black shale in Western Canada. *Earth Planet. Sci. Lett.* 222(3-4):729-740.
57. Ross GM, Bloch JD, & Krouse HR (1995) Neoproterozoic strata of the southern Canadian Cordillera and the isotopic evolution of seawater sulfate. *Precambrian Res.* 73(1-4):71-99.
58. King AF (1980) *The Birth of the Caledonides: Late Precambrian rocks of the Avalon Peninsula, Neowfoundland, and their correlative in the Appalachian Orogen* (Virginia Polytechnic Institute).
59. Narbonne GM, LaFlamme M. (2009) Neoproterozoic Glaciation, Oxygenation, and the Rise of Animals in Avalonian Newfoundland. in *Field Trip Guidebook* (NASA Astrobiology Institute).
60. Narbonne GM & Gehling JG (2003) Life after snowball: The oldest complex Ediacaran fossils. (Translated from English) *Geology* 31(1):27-30 (in English).

61. Canfield DE, Poulton SW, & Narbonne GM (2007) Late-Neoproterozoic deep-ocean oxygenation and the rise of animal life. (Translated from English) *Science* 315(5808):92-95 (in English).
62. Schröder S, Grotzinger, J.P. (2007) Evidence for anoxia at the Ediacaran-Cambrian boundary: the record of redox-sensitive trace elements and rare earth elements in Oman. . *Journal of the Geological Society, v. 164 p. 175-187*.
63. Bowring S*, et al.* (2007) Geochronologic constraints on the chronostratigraphic framework of the Neoproterozoic Huqf Supergroup, Sultanate of Oman. *Am. J. Sci.* 307(10):1097.
64. Lehmann B*, et al.* (2007) Highly metalliferous carbonaceous shale and Early Cambrian seawater. *Geology* 35:403-406.
65. Wille M, Nagler TF, Lehmann B, Schroder S, & Kramers JD (2008) Hydrogen sulphide release to surface waters at the Precambrian/Cambrian boundary. (Translated from English) *Nature* 453(7196):767-769 (in English).
66. Jiang SY*, et al.* (2009) Early Cambrian ocean anoxia in South China. (Translated from English) *Nature* 459(7248):E5-E6 (in English).
67. Mao J*, et al.* (2002) Re-Os dating of polymetallic Ni-Mo-PGE-Au mineralization in Lower Cambrian black shales of South China and its geologic significance. *Economic Geology* 97(5):1051-1061.
68. Steiner M, Wallis E, Erdtmann B-D, Zhao Y, & Yang R (2001) Submarine-hydrothermal exhalative ore layers in black shales from South China and associated fossils -- insights into a Lower Cambrian facies and bio-evolution. *Palaeogeography, Palaeoclimatology, Palaeoecology* 169(3-4):165-191.
69. Jiang S-Y*, et al.* (2007) Extreme enrichment of polymetallic Ni-Mo-PGE-Au in Lower Cambrian black shales of South China: An Os isotope and PGE geochemical investigation. *Palaeogeography, Palaeoclimatology, Palaeoecology* 254(1-2):217-228.
70. Luo KH, Jiang Z. W., Tang, L. D. (1994) Stratotype section for the Lower Cambrian stages in China. . *Kunming, China.* 1-183.
71. Zhu MY, Zhang, J. M., Li, G. X. (2001) Sedimentary environments of the Early Cambrian Chengjiang biota: Sedimentology of the Yu'anshan Formation in Chengjiang county, Eastern Yunnan. *Acta Palaeontologica Sinica* 40 (Sup):80-105.
72. Hu S (2005) Taphonomy and palaeoecology of the Early Cambrian Chengjiang Biota from eastern Yunnan, China. PhD).
73. Hou XG, Aldridge, R. J., Bergström, J., Siveter, D. J., Siveter, D. J., Feng., X. H. (2004) *The Cambrian fossils of Chengjiang, China - the flowering of early animal life* (Blackwell Publishing).
74. Babcock LE, Zhang, W., Leslie, S. A. (2001) The Chengjiang biota: Record of the Early Cambrian diversification of life and clues to exceptional preservation of fossils. *GSA Today* 11:4-9.
75. Hagadorn JW (2002) *Chengjiang: early record of the Cambrian explosion* (Columbia University Press) (English) pp 35-60.
76. Steiner M, Zhu M-Y, Weber B, & Geyer G (2001) The Lower Cambrian of Eastern Yunnan: Trilobite-based biostratigraphy and related faunas. (Translated from English) *Acta Palaeontologica Sinica* 40:63-79 (in English).

77. Jenkins RJF, Cooper JA, & Compston W (2002) Age and biostratigraphy of Early Cambrian tuffs from SE Australia and southern China. (Translated from English) *J. Geol. Soc.* 159:645-658 (in English).
78. Zang WL (1992) Sinian and Early Cambrian Floras and Biostratigraphy on the South China Platform. (Translated from English) *Palaeontographica Abteilung B Palaeophytologie* 224(4-6):75-119 (in English).
79. Zhang JM, Li, G. X., Zhou, C. M., Zhu, M. Y., Yu, Z. Y. (1997) Carbon isotope profiles and their correlation across the Neoproterozoic-Cambrian boundary interval on theYangtze Platform, China. *Bulletin of National Museum of Natural Science (Taiwan)* 10:107-116.
80. Hou X & Bergstrom J (1997) Arthropods of the Lower Cambrian Chengjiang fauna, southwest China. (Translated from English) *Fossils and Strata* 45:1-116 (in English).
81. Fletcher TP & Collins DH (1998) The Middle Cambrian Burgess Shale and its relationship to the Stephen Formation in the southern Canadian Rocky Mountains. (Translated from English) *Can. J. Earth Sci.* 35(4):413-436 (in English).
82. Morris S (1986) The community structure of the Middle Cambrian phyllopod bed(Burgess Shale). *Palaeontology* 29(3):423-467.
83. Powell WG, Johnston PA, & Collom CJ (2003) Geochemical evidence for oxygenated bottom waters during deposition of fossiliferous strata of the Burgess Shale Formation. *Palaeogeography, Palaeoclimatology, Palaeoecology* 201(3-4):249-268.
84. Lindstrom M (1971) Vom Anfang, Hochstand und Ende eines Epikontinental-Meeres. *Geologisches Rundschau* 60:419-438.
85. Thickpenny A (1984) The sedimentology of the Swedish alum shales. *Geological Society London Special Publications* 15(1):511.
86. Schovsbo N (2003) The geochemistry of Lower Palaeozoic sediments deposited on the margins of Baltica. *Bulletin of the Geological Society of Denmark* 50:11-27.
87. Henningsmoen G (1957) *The trilobite family Olenidae: with description of Norwegian material and remarks on the Olenid and Tremadocian series* (H. Aschehoug & Co.(Nygaard)).
88. Gradstein FM, Ogg JG, & van Kranendonk M (2008) On the geologic time scale 2008. (Translated from English) *Newsl. Stratigr.* 43(1):5-13 (in English).
89. Ahlberg P*, et al.* (2009) Cambrian high-resolution biostratigraphy and carbon isotope chemostratigraphy in Scania, Sweden: first record of the SPICE and DICE excursions in Scandinavia. *Lethaia* 42(1):2-16.
90. Schovsbo NH (2001) Why barren intervals? A taphonomic case study of the Scandinavian Alum Shale and its faunas. *Lethaia* 34(4):271-285.
91. Tjernvik T (1958) The Tremadocian beds at Flagabro in south-eastern Scania (Sweden). *Gff* 80(3):259-276.
92. Ekstrom G (1937) Upper Didymograptus Shale in Scania. in *Sveriges Geologiska Undersokning*), pp 1-53.
93. Maletz J (1995) The Middle Ordovician (Llanvirn) graptolite succession of the Albjara core (Scania, Sweden) and its implication for a revised zonation. *Zeitschrift für Geologische Wissenschaften* 23:249-259.

94. Bjerreskov M (1975) Llandoverian and Wenlockian Graptolites from Bornholm Denmark. *Fossils and Strata* (8):3-95.
95. Koren T & Bjerreskov M (1997) Early Llandovery monograptids from Bornholm and the southern Urals: taxonomy and evolution. *Bulletin of the Geological Society of Denmark* 44:1-43.
96. Cocks L (1985) The Ordovician-Silurian boundary. *Episodes* 8(2):98-100.
97. Holland C (1985) Series and stages of the Silurian System. *Episodes* 8:101-103.
98. Scotese C & McKerrow W (1990) Revised world maps and introduction. *Geological Society London Memoirs* 12(1):1.
99. Armstrong HA (1995) High-resolution biostratigraphy (conodonts and graptolites) of the Upper Ordovician and Lower Silurian - evaluation of the Late Ordovician mass extinction. (Translated from English) *Modern Geology* 20(1):41-68 (in English).
100. Brenchley P*, et al.* (1994) Bathymetric and isotopic evidence for a short-lived Late Ordovician glaciation in a greenhouse period. *Geology* 22(4):295.
101. Theron JN, Rickards RB, & Aldridge RJ (1990) Bedding-plane Assemblages of Promissum-Pulchrum - A New Giant Ashgill Conodont from the Table Mountain-Group, South Africa. (Translated from English) *Palaeontology* 33:577-594 (in English).
102. Elliot WL (1986) Siliciclastic shorelines. *Sedimentary environments and facies.* , ed Reading HG (Blackwell Scientific Publications, Oxford), pp 155-188.
103. Rust IC (1967) On the sedimentation of the Table Mountain Group in the Western Cape Province. D. Sc D. Sc Thesis (University of Stellenbosch, South Africa, Stellenbosch).
104. Hammarlund E (2007) Ocean chemistry at Cambrian deposits with exceptional preservation and the influence of sulfate on soft-tissue decay. M.Sc. Master's Thesis (University of Southern Denmark., Odense).
105. Tucker RD*, et al.* (1998) New U-Pb zircon ages and the duration and division of Devonian time. *Earth Planet. Sci. Lett.* 158(3-4):175-186.
106. Werne JP, Sageman BB, Lyons TW, & Hollander DJ (2002) An integrated assessment of a "type euxinic" deposit: Evidence for multiple controls on black shale deposition in the Middle Devonian Oatka Creek Formation. (Translated from English) *Am. J. Sci.* 302(2):110-143 (in English).
107. Kaufmann B (2006) Calibrating the Devonian Time Scale: A synthesis of U-Pb ID-TIMS ages and conodont stratigraphy. *Earth-Science Reviews* 76(3-4):175-190.
108. Sageman BB*, et al.* (2003) A tale of shales: the relative roles of production, decomposition, and dilution in the accumulation of organic-rich strata, Middle-Upper Devonian, Appalachian basin. *Chemical Geology* 195(1-4):229-273.
109. Murphy A, Sageman B, Hollander D, Lyons T, & Brett C (2000) Black shale deposition and faunal overturn in the Devonian Appalachian basin: Clastic starvation, seasonal water-column mixing, and efficient biolimiting nutrient recycling. *Paleoceanography* 15(3):280-291.
110. Over DJ, Lazar R, Baird GC, Schieber J, & Ettensohn FR (2009) Protosalvinia Dawson and Associated Conodonts of the Upper Trachytera Zone, Famennian,

Upper Devonian, in the United States. (Translated from English) *J. Paleontol.* 83(1):70-79 (in English).
111. Brown TC & Kenig F (2004) Water column structure during deposition of Middle Devonian-Lower Mississippian black and green/gray shales of the Illinois and Michigan Basins: a biomarker approach. (Translated from English) *Palaeogeography Palaeoclimatology Palaeoecology* 215(1-2):59-85 (in English).
112. Schieber J (2009) Discovery of agglutinated benthic foraminifera in Devonian black shales and their relevance for the redox state of ancient seas. (Translated from English) *Palaeogeography Palaeoclimatology Palaeoecology* 271(3-4):292-300 (in English).
113. Brown TC & Kenig F (2004) Water column structure during deposition of Middle Devonian-Lower Mississippian black and green/gray shales of the Illinois and Michigan Basins: a biomarker approach. *Palaeogeography, Palaeoclimatology, Palaeoecology* 215(1-2):59-85.
114. Schieber J & Lazar R (2004) Devonian Black Shales of the Eastern US: new insights into sedimentology and stratigraphy from the subsurface and outcrops in the Illinois and Appalachian Basins. pp 04-05.
115. Hallam A (1967) An environmental study of the upper Domerian and Lower Toarcian in Great Britain: Philosophical Transactions of the Royal Society of London, ser. *B* 252:393-445.
116. Hallam A (1975) *Jurassic environments* (Cambridge University Press Cambridge) p pp. 269.
117. Powell J (1984) Lithostratigraphical nomenclature of the Lias Group in the Yorkshire Basin. *Proceedings of the Yorkshire Geological Society* 45(1-2):51-57.
118. Jenkyns H (1985) The Early Toarcian and Cenomanian-Turonian anoxic events in Europe: comparisons and contrasts. *International Journal of Earth Sciences* 74(3):505-518.
119. Jenkyns H (1988) The early Toarcian (Jurassic) anoxic event; stratigraphic, sedimentary and geochemical evidence. *Am. J. Sci.* 288(2):101.
120. Hallam A (1962) A band of extraordinary calcareous concretion in the Upper Lias of Yorkshire, England. *Journal of Sedimentary Petrology* 32(4):840-847.
121. Howarth RJ (1962) The Jet Rock Series and the Alum Shale Series of the Yorkshire Coast. *Proceedings of the Yorkshire Geological Society* 33(18):381-422.
122. Morris K (1979) A classification of Jurassic marine shale squence: An example from the Toarcian (Lower Jurassic) of Great Britain. in *Palaeogeography, Palaeoclimatology, Palaeoecology*), pp 117-126.
123. Jenkyns HC & Clayton C (1997) Lower Jurassic epicontinental carbonates and mudstones from England and Wales: chemostratigraphic …. *Sedimentology* 44:687-706.
124. Wignall PB, Newton R, & Little CTS (2005) The timing of paleoenvironmental change and cause-and-effect relationships during the early Jurassic mass extinction in Europe. *Am. J. Sci* 305:1014-1032.
125. Raiswell R & Berner R (1985) Pyrite formation in euxinic and semi-euxinic sediments. *American Journal of Science* 285:710-724.

126. Bowden S, Farrimond P, Snape C, & Love GD (2006) Compositional differences in biomarker constituents of the hydrocarbon, resin, asphaltene and kerogen fractions: An example from the Jet Rock (Yorkshire, UK). *Organic Geochemistry* 37(3):369-383.
127. Mcarthur JM, Algeo TJ, van de Schootbrugge B, Li Q, & Howarth RJ (2008) Basinal restriction, black shales, Re-Os dating, and the Early Toarcian (Jurassic) oceanic anoxic event. *Paleoceangraphy* 23(4):22.
128. Pearce CR, Cohen AS, Coe AL, & Burton KW (2008) Molybdenum isotope evidence for global ocean anoxia coupled with perturbations to the carbon cycle during the early Jurassic. (Translated from English) *Geology* 36(3):231-234 (in English).